The 8th European Congress on Computational Methods in Applied Sciences and Engineering
ECCOMAS Congress 2022
5-–9 June 2022, Oslo, Norway

COMPARISON OF TWO ALTERNATIVE ENTROPY STABILIZATION TECHNIQUES FOR DISCONTINUOUS GALERKIN SPECTRAL ELEMENT METHODS

JOHANNES MARKERT* [1] **AND GREGOR J. GASSNER**[2]

[1] German Aerospace Center (DLR), Linder Höhe, 51147 Cologne, Germany,
johannes.markert@dlr.de, www.jmark.de

[2] Department for Mathematics and Computer Science; Center for Data and Simulation Science, University of Cologne, Weyertal 86-90, 50931, Cologne, Germany

Key words: Discontinuous Galerkin, Entropy Stability, Compressible Flows

Abstract. We review and compare two techniques to get entropy stability for nodal Discontinuous Galerkin Spectral Element Methods (DG) in compressible flows. One technique is based on entropy split-forms, e.g., [8, 15, 5] and one is based on a direct algebraic correction [1].

We have implemented the Flux Differencing methodology for both, Legendre-Gauss-Lobatto (Lobatto) and Legendre-Gauss (Gauss) based spectral element basis functions. While the Lobatto operators belong to the class of diagonal norm summation-by-parts (SBP) operators, the Gauss operators belong to the generalized class of SBP operators, where it is not necessary that the boundary nodes are included. To reach entropy stability, respectively guaranteed entropy dissipation, a key ingredient is an entropy conserving numerical flux function. With this ingredient, only the volume integral term of the DG method has to be modified accordingly.

We have also implemented an alternative technique, which is in general applicable for a wide range of discretizations. Abgrall [R. Abgrall, *A general framework to construct schemes satisfying additional conservation relations. Application to entropy conservative and entropy dissipative schemes.* Journal of Computational Physics, vol 372, 2018] introduced an algebraic correction term that retains conservation of the primary quantities and is furthermore constructed such, that an entropy (in-) equality can be shown. The second technique is at first sight a simpler alternative to the split-form based approach. Hence, questions regarding its advantages and disadvantages naturally come up.

1 INTRODUCTION

In engineering applications, Discontinuous Galerkin methods (DG) have been proven to be a powerful and flexible class of high order methods for the direct numerical simulation of turbulent flows in the low Mach regime. DG schemes can be interpreted as a mixture of high order Finite Element methods with local polynomial basis functions and Finite Volume methods, in the sense that the ansatz space is discontinuous across mesh element interfaces enabling the use of Riemann solvers based numerical surface fluxes [19, 18, 21]. High order DG methods are appreciated for their very low dispersion and dissipation errors, e.g., [2, 12]. Low numerical dissipation is

important to reduce artificial damping and heating, in addition, low dispersion errors are equally important as it guarantees high fidelity for wave propagation and wave interaction.

Driven by the success of DG in the engineering disciplines, a growing interest in the astrophysics community arises with the wish to apply high order DG to their problems. DG implementations with focus on astrophysical fluid dynamics and related applications are for instance presented in [25, 29, 3, 17]. In astrophysical simulations, irregular solutions are a common issue, since by today's standards most numerical models are gravely under-resolved considering the vast amount of scales in the Universe. However, high order DG methods are not renowned for their robustness [20, 22] regarding under-resolved flows. We consider a scheme robust when its behavior is verifiable and predictable for a broad range of flow configurations and the scheme is able to finish the simulation without crashing.

Making DG stable for under-resolved solutions without compromising the highly accurate wave propagation properties and losing its data locality is subject of current research and no "golden" way has been found so far. It is hoped that the key to universally robust high order methods are entropy stable (ES) schemes [9] faithfully obeying the second law of thermodynamics on a discrete level.

Abgrall [1] developed a general framework to construct numerical schemes satisfying additional conservation constraints, such as entropy conservation. Algebraic (anti-)diffusion-like terms correct the entropy erroneously produced/destructed by the numerical scheme at each timestep, making it another interesting - so far not broadly investigated - approach to achieve entropy stability for DG.

Provable entropy stable high order split-form DG schemes based on summation-by-part (SBP) operators [8, 14] allow to successfully stabilize unsteady flow simulations in engineering applications. Stabilized high order DG schemes are capable of directly simulating viscid, weakly compressible turbulence models with considerably elevated accuracy, at lower resolution and with better performance compared to traditional fluid solvers, e.g., [13, 4, 11, 10].

However, the successful application of high order DG for highly compressible, transonic to supersonic turbulence is still uncharted territory - a problem domain which is of great interest for applications especially in astrophysics. Hence, as a first step, we want to find out if we can successfully run high order DG in transonic compressible regimes for inviscid flows. We propose an initially smooth and subsonic weakly-magnetized Kelvin-Helmholtz-Instability (KHI) setup, which pushes a number of high order DG variants to their limits since locally the simulations develop challenging transonic flow configurations usually bringing un-stabilized high order schemes to a crash.

The structure of the rest of this article is as follows. In Section 2 we briefly introduce the governing equations together with a short discussion on their entropy relations. The investigated numerical schemes are reviewed in Section 3, where we introduce the concept of local surplus entropy production. In Section 4 we discuss the results regarding the scheme's performances of the aforementioned KHI simulations and Section 5 draws the conclusion.

2 GOVERNING EQUATIONS

We generally consider an initial value problem for hyperbolic partial differential equations (PDE) of the form

$$\partial_t \boldsymbol{u}(\vec{x},t) + \nabla \cdot \overleftrightarrow{\boldsymbol{F}}(\boldsymbol{u}(\vec{x},t)) = \boldsymbol{Q}(\boldsymbol{u}) \cdot \nabla \boldsymbol{u}, \quad \boldsymbol{u}(\vec{x},t=0) = \boldsymbol{u}_0(\vec{x}), \tag{1}$$

with the multivariate flux function $\overleftrightarrow{\boldsymbol{F}}$ depending only on the vector $\boldsymbol{u}$ of m state variables and an optional non-conservative PDE term $\boldsymbol{Q}(\boldsymbol{u}) \cdot \nabla \boldsymbol{u}$. Furthermore, we assume that the inviscid equations (1) are equipped with a family of entropy-entropy flux pairs $(\mathcal{S}, \vec{\mathcal{F}})$ adhering to the mathematical entropy inequality

$$\partial_t \mathcal{S}(\boldsymbol{u}(\vec{x},t)) + \nabla \cdot \vec{\mathcal{F}}(\boldsymbol{u}(\vec{x},t)) \leq 0, \tag{2}$$

which we understand in a weak sense. State flux $\overleftrightarrow{\boldsymbol{F}}$ and entropy flux $\vec{\mathcal{F}}$ are related by

$$\Big(\nabla_{\boldsymbol{u}} \vec{\mathcal{F}}(\boldsymbol{u})\Big)^T = \boldsymbol{w}^T \left(\nabla_{\boldsymbol{u}} \overleftrightarrow{\boldsymbol{F}}(\boldsymbol{u}) - \boldsymbol{Q}(\boldsymbol{u})\right) \tag{3}$$

with $\boldsymbol{w} = \nabla_{\boldsymbol{u}} \mathcal{S}(\boldsymbol{u})$ being the vector of m entropy variables and $\nabla_{\boldsymbol{u}} \overleftrightarrow{\boldsymbol{F}}$ being the usual flux Jacobians.

2.1 Ideal Generalized Lagrange Multiplier Magnetohydrodynamics

For our simulations we adopt the ideal generalized Lagrange multiplier magnetohydrodynamics (GLM-MHD) equations [7]

$$\partial_t \underbrace{\begin{pmatrix} \rho \\ \rho\,\vec{v} \\ E \\ \vec{B} \\ \Psi \end{pmatrix}}_{\boldsymbol{u}} + \nabla \cdot \underbrace{\begin{pmatrix} \rho\,\vec{v} \\ \rho\,\vec{v}\otimes\vec{v} + P\,\mathbb{1} - \vec{B}\otimes\vec{B} \\ (E+P)\vec{v} - (\vec{v}\cdot\vec{B} - c_{\mathrm{H}}\,\Psi)\vec{B} \\ \vec{B}\otimes\vec{v} - \vec{v}\otimes\vec{B} + c_{\mathrm{H}}\,\psi\,\mathbb{1} \\ c_{\mathrm{H}}\,\vec{B} \end{pmatrix}}_{\overleftrightarrow{\boldsymbol{F}}} = -(\nabla\cdot\vec{B}) \underbrace{\begin{pmatrix} 0 \\ \vec{B} \\ \vec{v}\cdot\vec{B} \\ \vec{v} \\ 0 \end{pmatrix}}_{\boldsymbol{\Phi}^{\mathrm{Powell}}} - (\nabla\Psi) \underbrace{\begin{pmatrix} \vec{0} \\ 0 \\ \vec{v}\,\Psi \\ 0 \\ \vec{v} \end{pmatrix}}_{\boldsymbol{\Phi}^{\mathrm{GLM}}}, \tag{4}$$

where ρ is the density, $\vec{v} = (v_1, v_2, v_3)^T$ is the velocity, E is the total energy, $\vec{B} = (B_1, B_2, B_3)^T$ is the magnetic field vector and Ψ is the hyperbolic divergence correction field. Note, we assumed the magnetic permeability to be $\mu_0 := 1$. $\mathbb{1}$ represents the 3×3 identity matrix and the total pressure P is the sum of thermal and magnetic pressure, i.e. $P = p + \frac{1}{2}\vec{B}^{\,2}$. The total energy E is related to the thermal pressure p via the equation-of-state

$$p = (\gamma - 1)\Big(E - \frac{\rho}{2}\vec{v}^{\,2} - \frac{1}{2}\vec{B}^{\,2} - \frac{1}{2}\Psi^2\Big), \tag{5}$$

where γ as the ratio of heat capacities for constant volume and pressure. If not stated otherwise, we set $\gamma = 5/3$. Furthermore, we identify the divergence correction speed c_{H} with the maximum wave speed $\lambda^{\max}$ given in [7]. The set of physically permissible states is defined by

$$\Pi = \big\{\text{permissible states}\big\} = \big\{\forall\, \boldsymbol{u} \;\big|\; \rho > 0 \wedge p(\boldsymbol{u}) > 0\big\}. \tag{6}$$

In order to symmetrize the system of equations (4), two non-conservative source terms are added, labeled Powell and GLM, which tend to zero in case of vanishing divergence error, i.e. $\nabla \cdot \vec{B} \to 0$. The family of entropy-entropy flux pairs is then of the form

$$\mathcal{S}(\boldsymbol{u}) = -\frac{\rho\, s}{\gamma - 1} \quad \text{and} \quad \vec{\mathcal{F}}(\boldsymbol{u}) = \mathcal{S}(\boldsymbol{u})\, \vec{v} \quad \text{with} \quad s = \log(p) - \gamma\, \log(\rho). \tag{7}$$

The corresponding entropy variables $\boldsymbol{w}$ are given by

$$\boldsymbol{w}(\boldsymbol{u}) = \left(\frac{\gamma - s}{\gamma - 1} - \beta\, \vec{v}^2,\ 2\,\beta\, \vec{v}^T,\ -2\,\beta,\ 2\,\beta\, \vec{B}^T,\ 2\,\beta\, \Psi \right)^T \quad \text{with} \quad \beta = \frac{\rho}{2\,p}. \tag{8}$$

The entropy potential $\vec{\theta}$ is given by

$$\vec{\theta} = \rho\, \vec{v} + \beta\, \vec{B}^{\,2}\, \vec{v} + 2\,\beta\, c_{\mathrm{H}}\, \Psi\, \vec{B}. \tag{9}$$

We refer to [7] for the detailed entropy analysis.

3 NUMERICAL SCHEME

3.1 Collocation Scheme

We briefly outline the construction of the Discontinuous Galerkin Spectral Element Method (DGSEM) in 2D. Detailed derivations can be found for example in [21]. Here, we use DG and DGSEM synonymously. To derive the N-th order 2D DG scheme within Q non-overlapping elements $\Omega_q \subset \Omega$ of the Cartesian domain $\Omega \subset \mathbb{R}^2$, we start with the general hyperbolic PDE (1) and omit the non-conservative terms for now. For the variational form, we multiply by the test function $\phi(\vec{\chi})$, apply integration-by-parts in space and transform to the reference element $\vec{\chi} \in \mathcal{I}^2 = \left[-\frac{1}{2}, \frac{1}{2}\right]^2$. We get

$$|\Omega_q| \int_{\mathcal{I}^2} \left(\partial_t \boldsymbol{u}(\vec{\chi}, t)\right) \phi(\vec{\chi})\, \mathrm{d}\vec{\chi} = \int_{\mathcal{I}^2} \overleftrightarrow{\boldsymbol{F}}(\boldsymbol{u}(\vec{\chi}, t))\, \nabla\phi(\vec{\chi})\, \mathrm{d}\vec{\chi} - \oint_{\partial\mathcal{I}^2} \overleftrightarrow{\boldsymbol{F}}(\boldsymbol{u}(\vec{\chi}, t))\, \phi(\vec{\chi})\, \vec{n}(\vec{\chi})\, \mathrm{d}(\partial\mathcal{I}^2) \tag{10}$$

with the outward facing normal vector $\vec{n}(\vec{\chi})$ and the element volume $|\Omega_q| = \Delta x \Delta y$. Next, we identify the test function with the Lagrange polynomials, i.e. $\phi(\vec{\chi}) := \ell_i(\vec{\chi})$, which allows us to conveniently construct the so-called DG operators for quadrature, differentiation and boundary evaluation:

$$\boldsymbol{M}_{ij} := \delta_{i,j}\, \omega_i \overset{\text{lump}}{\approx} \int_{\mathcal{I}} \ell_j(\chi)\ell_i(\chi)\, \mathrm{d}\chi,\ \boldsymbol{D}_{ij} := \partial_\chi \ell_j(\chi)\big|_{\xi_i},\ \boldsymbol{B}_i^{\pm} := \ell_i\left(\pm\frac{1}{2}\right),\ i,j = 1 \ldots N. \tag{11}$$

If we make the polynomial tensor product ansatz with N interpolation nodes $\xi_i \in \mathcal{I}$, $\boldsymbol{u}(\vec{\chi}) \approx \sum_{i,j,k=1}^{N} \boldsymbol{u}(\vec{\chi})\, \ell_i(\chi_1)\ell_j(\chi_2)$, and collocate quadrature and interpolation, we get the semi-discrete weak-form DG scheme:

$$\begin{aligned} \dot{\boldsymbol{u}}_{ij} = &- \frac{1}{\omega_i\, \Delta x}\Big(\boldsymbol{B}_j^{+}\, (\boldsymbol{F}_x^*)_j^{+} - \boldsymbol{B}_j^{-}\, (\boldsymbol{F}_x^*)_j^{-} - \sum_{l=1}^{N} \omega_l\, \boldsymbol{D}_{li}\, (\boldsymbol{F}_x)_{lj} \Big) \\ &- \frac{1}{\omega_j\, \Delta y}\Big(\boldsymbol{B}_i^{+}\, (\boldsymbol{F}_y^*)_i^{+} - \boldsymbol{B}_i^{-}\, (\boldsymbol{F}_y^*)_i^{-} - \sum_{l=1}^{N} \omega_l\, \boldsymbol{D}_{lj}\, (\boldsymbol{F}_y)_{il} \Big) - \boldsymbol{\Upsilon}_{ij} \end{aligned} \tag{12}$$

with volume fluxes $\boldsymbol{F}_{x|y} = \overleftrightarrow{\boldsymbol{F}}_{x|y}(\boldsymbol{u})$ and numerical fluxes $(\boldsymbol{F}^*_{x|y})^{\pm} = \boldsymbol{F}^*_{x|y}(\boldsymbol{u}^{\pm}_{\mathrm{L}}, \boldsymbol{u}^{\pm}_{\mathrm{R}})$. The inner element boundaries in x-direction read $\boldsymbol{u}^{\pm}_j = \sum_{i=1}^N \boldsymbol{B}^{\pm}_i \boldsymbol{u}_{ij}$ and in y-direction $\boldsymbol{u}^{\pm}_i = \sum_{j=1}^N \boldsymbol{B}^{\pm}_j \boldsymbol{u}_{ij}$. In this work, we use Legendre-Gauss (Gauss) and Legendre-Gauss-Lobatto (Lobatto) collocation nodes.

We added the non-conservative source terms $\boldsymbol{\Upsilon} = -\boldsymbol{\Upsilon}^{\mathrm{Powell}} - \boldsymbol{\Upsilon}^{\mathrm{GLM}}$, which are analogously discretized by the DG approach (see, e.g., [27] for details):

$$\boldsymbol{\Upsilon}^{\mathrm{Powell}}_{ij} = \left(\frac{1}{\omega_i \, \Delta x} \Big(\boldsymbol{B}^+_j \, \{\!\{B_1\}\!\}^+_j - \boldsymbol{B}^-_j \, \{\!\{B_1\}\!\}^-_j - \sum_{l=1}^N \omega_l \, \boldsymbol{D}_{li} \, (B_1)_{lj} \Big) + \frac{1}{\omega_j \, \Delta y} \Big(\dots \Big) \right) \boldsymbol{\Phi}^{\mathrm{Powell}}_{ij}, \tag{13}$$

$$\boldsymbol{\Upsilon}^{\mathrm{GLM}}_{ij} = \left(\frac{(v_1)_{ij}}{\omega_i \, \Delta x} \Big(\boldsymbol{B}^+_j \, \{\!\{\Psi\}\!\}^+_j - \boldsymbol{B}^-_j \, \{\!\{\Psi\}\!\}^-_j - \sum_{l=1}^N \omega_l \, \boldsymbol{D}_{li} \, \Psi_{lj} \Big) + \frac{(v_2)_{ij}}{\omega_j \, \Delta y} \Big(\dots \Big) \right) \boldsymbol{\Phi}^{\mathrm{GLM}}_{ij}. \tag{14}$$

The element interface averages read $\{\!\{\cdot\}\!\}^{\pm} = \frac{1}{2} \left((\cdot)^{\pm}_{\mathrm{L}} + (\cdot)^{\pm}_{\mathrm{R}} \right)$. The terms implied by "..." for the y-direction are constructed analogously to the x-direction and were left out for brevity.

For time integration we use an explicit strong-stability preserving, fourth order Runge-Kutta scheme (SSP-RK(5,4)) [16]. A stable timestep Δt is estimated by the usual CFL condition as

$$\Delta t := \frac{CFL}{d} \min_q^Q \frac{\min(\Delta x_q, \Delta y_q)}{N \, \lambda^{\max}_q}, \tag{15}$$

where $d = 2, CFL := 0.4$, N is the number of quadrature nodes in each direction in the element, and $\lambda^{\max}_q$ is the maximum wave speed estimate for the equations (4) in element q.

3.2 Surplus Entropy Production

In physics, entropy production arises from transfer processes across system boundaries, such as friction (viscosity), heat exchange, and matter diffusion. But also numerical schemes produce entropy via their inherent numerical diffusion. Suppose we have a semi-discretization $\dot{\boldsymbol{u}}$ of our conservation law (1) and by the same discretization mechanism we can derive an entropy residual $\dot{\mathcal{S}}$ measuring the correct entropy exchange rate across element boundaries $\partial\Omega_q$. The numerical scheme's contribution to the local entropy production at time t is then given by the surplus entropy production rate

$$\underbrace{\dot{\Delta\mathcal{S}}(t)\Big|_{\Omega_q}}_{\text{surplus entropy prod.}} = \underbrace{\boldsymbol{w}(t) \cdot \dot{\boldsymbol{u}}(t)\Big|_{\Omega_q}}_{\text{local entropy prod.}} - \underbrace{\dot{\mathcal{S}}(t)\Big|_{\partial\Omega_q}}_{\text{entropy exchange}}. \tag{16}$$

For our 2D DG scheme (12) the entropy exchange rate $\dot{\mathcal{S}}$ reads

$$\dot{\mathcal{S}}_{ij} = -\frac{1}{\omega_i \, \Delta x} \Big(\boldsymbol{B}^+_j \, (\mathcal{F}^*_x)^+_j - \boldsymbol{B}^-_j \, (\mathcal{F}^*_x)^-_j \Big) - \frac{1}{\omega_j \, \Delta y} \Big(\boldsymbol{B}^+_i \, (\mathcal{F}^*_y)^+_i - \boldsymbol{B}^-_i \, (\mathcal{F}^*_y)^-_i \Big) \tag{17}$$

with entropy projected numerical entropy fluxes $(\mathcal{F}^*_{x|y})^{\pm} = \mathcal{F}^*_{x|y}(\widetilde{\boldsymbol{u}}^{\pm}_{\mathrm{L}}, \widetilde{\boldsymbol{u}}^{\pm}_{\mathrm{R}})$. States at inner element boundaries, for example in x-direction, are computed as $\widetilde{\boldsymbol{u}}^{\pm}_j = \boldsymbol{u}\big(\sum_{i=1}^N \boldsymbol{B}^{\pm}_i \, \boldsymbol{w}(\boldsymbol{u}_{ij}) \big)$. Of

course, for quadrature rules with nodes at boundaries, e.g. Lobatto quadrature, the entropy projection step is not necessary.

The numerical entropy flux for system (4) is given by

$$\boldsymbol{\mathcal{F}}^*(\boldsymbol{u}_\mathrm{L}, \boldsymbol{u}_\mathrm{R}) = \{\!\{\boldsymbol{w}\}\!\} \cdot \boldsymbol{F}(\boldsymbol{u}_\mathrm{L}, \boldsymbol{u}_\mathrm{R}) - \{\!\{\theta\}\!\} + \frac{1}{2}\Big(\boldsymbol{w}_\mathrm{L} \cdot \boldsymbol{\Upsilon}(\boldsymbol{u}_\mathrm{L}, \boldsymbol{u}_\mathrm{R}) + \boldsymbol{w}_\mathrm{R} \cdot \boldsymbol{\Upsilon}(\boldsymbol{u}_\mathrm{R}, \boldsymbol{u}_\mathrm{L})\Big) \tag{18}$$

with the non-conservative two-point source term

$$\boldsymbol{\Upsilon}(\boldsymbol{u}_\mathrm{L}, \boldsymbol{u}_\mathrm{R}) = \{\!\{B\}\!\}\, \boldsymbol{\Phi}^{\mathrm{Powell}}(\boldsymbol{u}_\mathrm{L}) + v_\mathrm{L}\ \{\!\{\Psi\}\!\}\, \boldsymbol{\Phi}^{\mathrm{GLM}}(\boldsymbol{u}_\mathrm{L}). \tag{19}$$

Note, we purposely omitted any $(\cdot)^\pm$ to avoid notational clutter.

The local surplus entropy production rate per element is finally computed by summing over all nodes, i.e.

$$\overline{\dot{\Delta\mathcal{S}}} = \sum_{ij=1}^{N} \Big(\boldsymbol{w}_{ij} \cdot \dot{\boldsymbol{u}}_{ij}\ -\ \dot{\mathcal{S}}_{ij}\Big)\, \omega_i\, \omega_j. \tag{20}$$

Obviously, above surplus element production rate must always give zero or negative results, $\overline{\dot{\Delta\mathcal{S}}} \leq 0$, in order to fulfill the entropy inequality (2). However, we cannot deduce if the measured amount of surplus entropy (besides the sign) is adequate in any physical or numerical sense.

3.3 Provable Entropy Stable Schemes

Ensuring the correct sign of entropy production, namely entropy dissipation, is a crucial property of any numerical scheme. Our derived Standard DG scheme (12) does not necessarily fulfill the entropy inequality. Hence, additional modifications are required in order to achieve provable entropy dissipation, resp. entropy stability. In the following, we briefly introduce two different paths for such a modification.

The first approach is to correct any spurious entropy increase with an algebraic correction term by subtracting surplus entropy production in a conservative and entropy consistent manner. We coin this approach Entropy Corrected DG. The second approach is called Flux Differencing DG and builds on the (generalized) SBP property of the DG differentiation operator.

3.3.1 Entropy Corrected DG

The algebraic correction approach is introduced in [1] for a broad range of numerical schemes. The idea is intuitive, applicable for a wide class of equations, and is straightforward to implement. Key element is to find a correction term $\boldsymbol{r}$ if subtracted from the residual of the standard scheme, i.e.

$$\dot{\boldsymbol{u}}' = \dot{\boldsymbol{u}} - \boldsymbol{r}, \tag{21}$$

such that $\dot{\boldsymbol{u}}'$ satisfies the element entropy inequality (20), but does not break primary conservation. The two requirements define a linear system with always at least two unknowns. The algebraic solution, according to [1], reads

$$\boldsymbol{r}_{ij} = \frac{\boldsymbol{w}_{ij} - \overline{\boldsymbol{w}}}{\epsilon + \sum_{kl=1}^{N} (\boldsymbol{w}_{kl} - \overline{\boldsymbol{w}})^2\, \omega_k\, \omega_l}\ \max\Big(0, \overline{\dot{\Delta\mathcal{S}}}\Big) \tag{22}$$

with $\overline{\boldsymbol{w}} = \sum_{ij=1}^{N} \boldsymbol{w}_{ij}\,\omega_i\,\omega_j$ and the element entropy production rate $\overline{\dot{\Delta\mathcal{S}}}$ given by (20). The correction term (22) is conservative. The parameter $\epsilon := 10^{-20}$ prevents division by zero in case of constant states.

3.3.2 Flux Differencing DG

Chan et al. [5] introduced a provable entropy stable DG scheme for general quadrature rules based on the construction of generalized SBP operators [26]. Based on our DG operators (11) they read

$$(\boldsymbol{D}\,\boldsymbol{M}) + (\boldsymbol{D}\,\boldsymbol{M})^T = \left(\boldsymbol{B}^-|\boldsymbol{B}^+\right) \begin{pmatrix} -1 & 0 \\ 0 & 1 \end{pmatrix} \left(\boldsymbol{B}^-|\boldsymbol{B}^+\right)^T \tag{23}$$

where $(\boldsymbol{B}^-|\boldsymbol{B}^+) \in \mathbb{R}^{N\times 2}$ is the matrix of the two boundary evaluation operators in (11). The SBP property is a direct restatement of integration-by-parts in the continuous case. Equipped with relation (23), the the semi-discrete, weak-form DG (12) is rearranged as follows:

$$\dot{\boldsymbol{u}}_{ij} = -\frac{1}{\omega_i\,\Delta x}\Big(\boldsymbol{B}_j^+\,(\boldsymbol{F}_x^{\%})_{ij}^{\pm} - \boldsymbol{B}_i^-\,(\boldsymbol{F}_x^{\%})_{ij}^{\pm} - \sum_{l=1}^{N} \boldsymbol{S}_{li}\,(\boldsymbol{F}_x^{\#})_{\{l,i\}j}\Big) - \frac{1}{\omega_j\,\Delta y}\Big(\dots\Big) \tag{24}$$

where $\boldsymbol{S} = \boldsymbol{D}\,\boldsymbol{M} - (\boldsymbol{D}\,\boldsymbol{M})^T$ is the skew-symmetric flux differencing matrix and the volume flux operation is a telescopic sum defined by $\sum_{l=1}^{N} \boldsymbol{S}_{li}\,(\boldsymbol{F}_x^{\#})_{\{l,i\}j} = \sum_{l=1}^{N} \boldsymbol{S}_{li}\,\boldsymbol{F}_x^{\#}\big(\boldsymbol{u}_{lj}, \boldsymbol{u}_{ij}\big)$. The terms implied by "..." for the y-direction are constructed analogously to the x-direction and were left out for brevity. The special surface flux reads

$$(\boldsymbol{F}_x^{\%})_{ij}^{\pm} = \boldsymbol{F}_x^{*}\big((\widetilde{\boldsymbol{u}}_{\mathrm{L}}^{\pm})_j, (\widetilde{\boldsymbol{u}}_{\mathrm{R}}^{\pm})_j\big) + \boldsymbol{F}_x^{\#}\big(\widetilde{\boldsymbol{u}}_j^{\pm}, \boldsymbol{u}_{ij}\big) - \sum_{l=1}^{N} \boldsymbol{B}_l^{\pm}\,\boldsymbol{f}_x^{\#}\big(\widetilde{\boldsymbol{u}}_j^{\pm}, \boldsymbol{u}_{lj}\big), \tag{25}$$

where as before the terms at boundaries are evaluated on entropy projected states.

To obtain a provable entropy stable scheme for our system (4) we use the kinetic energy preserving and entropy conservative (KEPEC) numerical flux function given in [7] as the central-like base flux both for the volume flux $\boldsymbol{f}^{\#} := \boldsymbol{f}^{\mathrm{KEPEC}}$ and for the surface flux $\boldsymbol{f}^{*} := \boldsymbol{f}^{\mathrm{KEPEC}} - \Delta_{\mathrm{Rusanov}}$ with added Rusanov-type dissipation. The non-conservative two-point source term (19) is integrated by simply extending $\boldsymbol{f}^{\mathrm{KEPEC}}$ as follows [28]: $\boldsymbol{f}^{\mathrm{KEPEC}}\big(\boldsymbol{u}_{\mathrm{L}}, \boldsymbol{u}_{\mathrm{R}}\big) \to \boldsymbol{f}^{\mathrm{KEPEC}}\big(\boldsymbol{u}_{\mathrm{L}}, \boldsymbol{u}_{\mathrm{R}}\big) + \boldsymbol{\Upsilon}\big(\boldsymbol{u}_{\mathrm{L}}, \boldsymbol{u}_{\mathrm{R}}\big)$.

It is important to note that in the case of Lobatto collocation nodes, the generalized Flux Differencing scheme (24) reduces to the commonly known Flux Differencing scheme with diagonal-norm SBP operators with a lot less computational overhead.

4 ROBUSTNESS INVESTIGATION

For the stress test of the aforementioned entropy stable DG schemes we devised our own weakly-magnetized 2D MHD Kelvin-Helmholtz (KHI) instability setup [23]. This setup has proven to be useful for our purposes since it starts with a smooth well resolved initial state and gradually develops vortical, turbulent-like structures with increasingly smaller scales. Although, the setup is generally subsonic, it locally develops transonic regions, which are very challenging for the investigated schemes.

The weakly-magnetized 2D MHD KHI setup is initialized in a squared and periodic domain $\Omega = [-1, 1]^2$ and reads

$$\begin{aligned} \rho_0(\vec{x}) &= \frac{1}{2} + \frac{3}{4}\left(\tanh(15\,(y+\frac{1}{2})) - \tanh(15\,(y-\frac{1}{2}))\right) \\ (v_1)_0(\vec{x}) &= \frac{1}{2}\left(\tanh(15\,(y+\frac{1}{2})) - \tanh(15\,(y-\frac{1}{2})) + 1\right) \\ (v_2)_0(\vec{x}) &= \frac{1}{10}\,\sin(2\,\pi\,x),\ (v_3)_0 = 0,\ p_0 = 1,\ \vec{B}_0 = (10^{-2}, 0, 0)^T, \Psi_0 = 0. \end{aligned} \tag{26}$$

We compute the setup (26) with six variants of fourth order ($N = 4$) DG schemes: Standard DG, Entropy Corrected DG, and Flux Differencing DG each with Lobatto and Gauss collocation nodes. They are also listed in Table 1. Besides the two Standard DG variants, all schemes are provably entropy stable. Explicit time-stepping is carried out with the SSP-RK(5,4) [16] method. We let the simulations run on a uniform grid of 128^2 elements á 4^2 nodes till final time $T = 10$. Most schemes, however, crash beforehand, which we identify by the occurrence of nonphysical data according to the permissible set of states given in (6). All schemes have been implemented and run within the open source CFD framework NEMO [24] written in modern Fortran.

In Figure 1 we plot the minimum and maximum surplus element entropy production rates (20) in the whole computational domain Ω over simulation time t for all six investigated schemes. Clearly, both Standard DG variants reveal spurious positive production rates (dashed lines) and are the least robust schemes since they crash first at around $t \approx 3.2$. Curiously, the emergence of an unstable condition eventually leading to a crash is accompanied by extreme volatility in entropy production. Entropy correction according to (21) successfully suppresses any spurious entropy increase in the whole domain and at all times. Especially the variant with Gauss quadrature becomes substantially more robust keeping the simulation running well over $t > 5$. On the other hand, the Lobatto DG variant does not show significantly increased robustness compared to Standard DG and crashes at $t \approx 3.5$. A similar conclusion can also be drawn for the Flux Differencing DG scheme with Lobatto quadrature. Contrarily, Flux Differencing with Gauss quadrature is robust enough to successfully complete the simulation at final simulation time.

All results are compactly summarized in Table 1, where we also compare the elapsed runtimes the schemes consumed on a single compute core (serial execution) in order to reach simulation time $t = 2.5$. Our baseline is also the fastest scheme, namely the Standard DG with Lobatto quadrature, closely followed by the Standard DG with Gauss nodes. The costs of Entropy Correction amounts to a reasonable increase of up to 80% in runtime while Flux Differencing is a couple of times more expensive than the baseline. The biggest contribution to the runtime costs for the Flux Differencing schemes are the repeated evaluations (telescopic sums) of the rather expensive entropy conservative KEPEC flux, especially for the Gauss variant with its tight coupling of the surface fluxes with the inner states.

Table 1: Results of the robustness investigation for the six investigated DG variants simulating the 2D MHD-KHI setup (26). The second column lists the time of crash according to the settings described in the text while the third column compares the elapsed runtimes to reach simulation time $t = 2.5$. The benchmark was carried out with a uniform grid of 64^2 elements on a single compute core (#core = 1). All simulations took a total number of iteration steps of #steps $= 1263 \times 5$ (SSP-RK(5,4)). The performance measure throughput (TP) is defined as TP = (#steps $\times$ DOF)/(#cores $\times$ runtime).

numerical scheme	time of crash	runtime [s]	TP [10^6 DOF/s]	slowdown
Std. DG (Lobatto)	3.1	72.652	5.696	1.00
Std. DG (Gauss)	3.2	100.143	4.132	1.38
Entr. Corr. DG (Lobatto)	3.45	108.929	3.799	1.50
Entr. Corr. DG (Gauss)	5.3	131.164	3.155	1.80
Flux Diff. DG (Lobatto)	3.5	209.307	1.977	2.88
Flux Diff. DG (Gauss)	>10	435.082	0.951	6.00

5 CONCLUSION

We have briefly derived a nodal collocation DG method for the ideal GLM-MHD equations with special focus on the entropy balance. In order to ensure provable entropy dissipation we introduced two alternative entropy stabilization techniques, namely, Entropy Correction and Flux Differencing, which we investigated with regard to their robustness in simulating a two dimensional weakly-magnetized KHI setup. Although the setup is initially smooth and subsonic it gradually develops transonic regions of high compressibility. Such flow features are known to be a challenge for high order schemes of low dissipation. Entropy stabilization is considered a promising path towards improved robustness in such scenarios. In order to quantify and also to check the correct sign of the local entropy production we introduced the concept of surplus element entropy production.

Furthermore, we investigated the Standard DG variants with Lobatto and Gauss quadrature rules as well as their entropy stabilization via the two aforementioned approaches. All DG variants were fixed to fourth order in spatial accuracy and not "repaired" by any limiters such as lifting states a-posteriori into positivity. We observed that all DG variants with Lobatto quadrature rule are unacceptably fragile for these kind of simulations. Entropy stable DG schemes with Gauss quadrature rules, on the other hand, are noticeably more robust.

The Entropy Correction for Gauss DG is provable entropy stable and significantly increased the robustness in our tests. But it eventually crashed before reaching the final simulation time. One possible explanation might be the un-boundedness of the algebraic correction terms adding forceful source terms to the residual in case of challenging flow conditions. This might lead to a very stiff system, whose eigenvalues lie beyond the stability region of our applied explicit Runge-Kutta scheme. The entropy stable Flux Differencing DG with Gauss quadrature is the only unlimited DG variant capable to successfully finish our stress test simulation, which is remarkable! Chan et al. [6] gives further insights into the robustness properties of this scheme.

Apparently, Flux Differencing is two to three times more expensive than the algebraic correction approach. Hence, an interesting direction for future research might be to investigate the robustness properties of Entropy Correction for weakly compressible turbulence simulations as

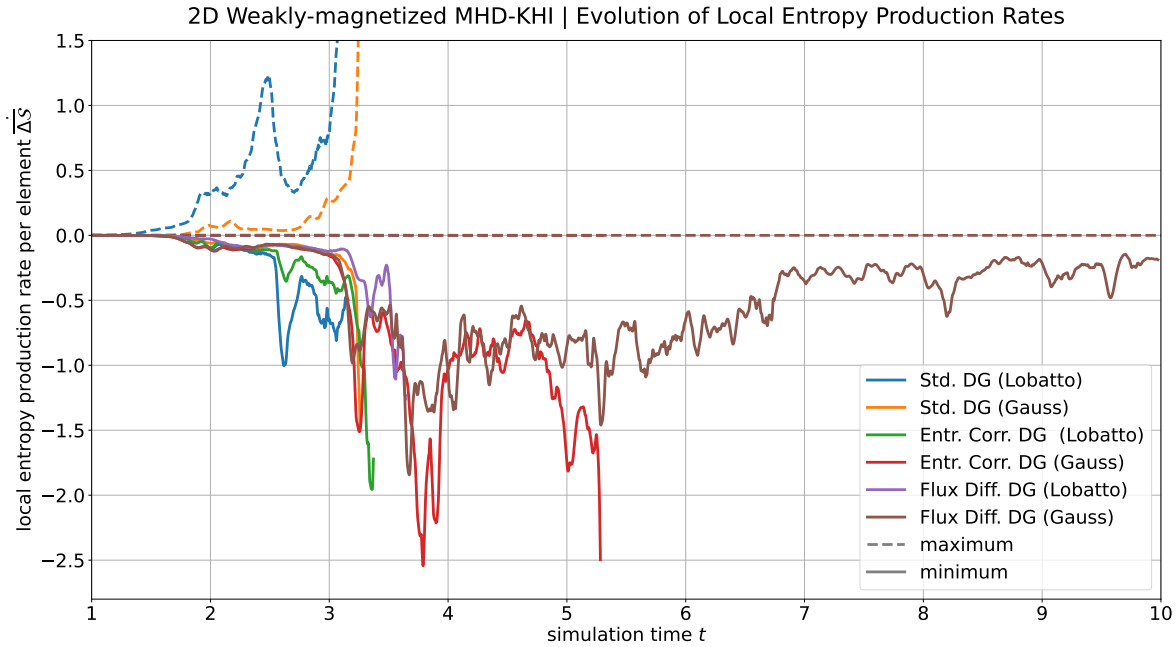

Figure 1: Evolution of minimum (solid lines) and maximum (dashed lines) surplus entropy production rates computed by the six investigated DG variants for the weakly-magnetized MHD-KHI setup (26).

already done extensively for entropy stable Flux Differencing schemes.

REFERENCES

[1] Remi Abgrall. A general framework to construct schemes satisfying additional conservation relations. application to entropy conservative and entropy dissipative schemes. *Journal of Computational Physics*, 372:640–666, 2018.

[2] Mark Ainsworth. Dispersive and dissipative behaviour of high order discontinuous galerkin finite element methods. *Journal of Computational Physics*, 198(1):106–130, 2004.

[3] Andreas Bauer, Kevin Schaal, Volker Springel, Praveen Chandrashekar, Rüdiger Pakmor, and Christian Klingenberg. Simulating turbulence using the astrophysical discontinuous galerkin code tenet. In *Software for Exascale Computing-SPPEXA 2013-2015*, pages 381–402. Springer, 2016.

[4] Andrea D. Beck, Thomas Bolemann, David Flad, Hannes Frank, Gregor J. Gassner, Florian Hindenlang, and Claus-Dieter Munz. High-order discontinuous galerkin spectral element methods for transitional and turbulent flow simulations. *International Journal for Numerical Methods in Fluids*, 76(8):522–548, 2014.

[5] Jesse Chan, David C Del Rey Fernández, and Mark H Carpenter. Efficient entropy stable gauss collocation methods. *SIAM Journal on Scientific Computing*, 41(5):A2938–A2966, 2019.

[6] Jesse Chan, Hendrik Ranocha, Andres Rueda-Ramirez, Gregor Gassner, and Tim Warburton. On the entropy projection and the robustness of high order entropy stable discontinuous galerkin schemes for under-resolved flows. *arXiv preprint arXiv:2203.10238*, 2022.

[7] Dominik Derigs, Andrew R Winters, Gregor J Gassner, Stefanie Walch, and Marvin Bohm. Ideal glm-mhd: About the entropy consistent nine-wave magnetic field divergence diminishing ideal magnetohydrodynamics equations. *Journal of Computational Physics*, 364:420–467, 2018.

[8] T.C. Fisher and M.H. Carpenter. High-order entropy stable finite difference schemes for nonlinear conservation laws: Finite domains. *Journal of Computational Physics*, 252:518–557, 2013.

[9] Ulrik S Fjordholm, Siddhartha Mishra, and Eitan Tadmor. Arbitrarily high-order accurate entropy stable essentially nonoscillatory schemes for systems of conservation laws. *SIAM Journal on Numerical Analysis*, 50(2):544–573, 2012.

[10] David Flad and Gregor Gassner. On the use of kinetic energy preservaing DG-scheme for large eddy simulation. *Journal of Computational Physics*, 350:782–795, 2017.

[11] Anirban Garai, Laslo Diosady, Scott Murman, and Nateri Madavan. Dns of flow in a low-pressure turbine cascade using a discontinuous-galerkin spectral-element method. In *Turbo Expo: Power for Land, Sea, and Air*, volume 56642, page V02BT39A023. American Society of Mechanical Engineers, 2015.

[12] Gregor Gassner and David A Kopriva. A comparison of the dispersion and dissipation errors of gauss and gauss–lobatto discontinuous galerkin spectral element methods. *SIAM Journal on Scientific Computing*, 33(5):2560–2579, 2011.

[13] Gregor J. Gassner and Andrea D. Beck. On the accuracy of high-order discretizations for underresolved turbulence simulations. *Theoretical and Computational Fluid Dynamics*, 27(3–4):221–237, 2013.

[14] Gregor J. Gassner, Andrew R. Winters, Florian J. Hindenlang, and David A. Kopriva. The BR1 scheme is stable for the compressible Navier–Stokes equations. *Journal of Scientific Computing*, Apr 2018.

[15] Gregor J Gassner, Andrew R Winters, and David A Kopriva. Split form nodal discontinuous galerkin schemes with summation-by-parts property for the compressible euler equations. *Journal of Computational Physics*, 327:39–66, 2016.

[16] Sigal Gottlieb, Chi-Wang Shu, and Eitan Tadmor. Strong stability-preserving high-order time discretization methods. *SIAM review*, 43(1):89–112, 2001.

[17] Thomas Guillet, Rüdiger Pakmor, Volker Springel, Praveen Chandrashekar, and Christian Klingenberg. High-order magnetohydrodynamics for astrophysics with an adaptive mesh refinement discontinuous galerkin scheme. *Monthly Notices of the Royal Astronomical Society*, 485(3):4209–4246, 2019.

[18] Jan S Hesthaven and Tim Warburton. *Nodal discontinuous Galerkin methods: algorithms, analysis, and applications*. Springer Science & Business Media, 2007.

[19] George Em Karniadakis, George Karniadakis, and Spencer Sherwin. *Spectral/hp element methods for computational fluid dynamics*. Oxford University Press on Demand, 2005.

[20] Robert M Kirby and Spencer J Sherwin. Aliasing errors due to quadratic nonlinearities on triangular spectral/hp element discretisations. *Journal of engineering mathematics*, 56(3):273–288, 2006.

[21] David A Kopriva. *Implementing spectral methods for partial differential equations: Algorithms for scientists and engineers*. Springer Science & Business Media, 2009.

[22] Juan Manzanero, Gonzalo Rubio, Esteban Ferrer, Eusebio Valero, and David A Kopriva. Insights on aliasing driven instabilities for advection equations with application to gauss–lobatto discontinuous galerkin methods. *Journal of Scientific Computing*, 75(3):1262–1281, 2018.

[23] J. Markert. Discontinuous galerkin spectral element methods for astrophysical flows in multi-physics applications. https://kups.ub.uni-koeln.de/61694, 2022.

[24] J. Markert. Nemo: 2D/3D CFD code. https://github.com/jmark/nemo, 2022.

[25] Philip Mocz, Mark Vogelsberger, Debora Sijacki, Rüdiger Pakmor, and Lars Hernquist. A discontinuous galerkin method for solving the fluid and magnetohydrodynamic equations in astrophysical simulations. *Monthly Notices of the Royal Astronomical Society*, 437(1):397–414, 2014.

[26] Hendrik Ranocha. *Generalised summation-by-parts operators and entropy stability of numerical methods for hyperbolic balance laws*. Cuvillier Verlag, 2018.

[27] Andrés M Rueda-Ramírez, Sebastian Hennemann, Florian J Hindenlang, Andrew R Winters, and Gregor J Gassner. An entropy stable nodal discontinuous galerkin method for the resistive mhd equations. part ii: Subcell finite volume shock capturing. *Journal of Computational Physics*, 444:110580, 2021.

[28] Andrés M Rueda-Ramírez, F. J Hindenlang, and Gregor J Gassner. Entropy-stable gauss collocation methods for ideal magnetohydrodynamics. *arXiv preprint arXiv:2203.06062*, 2022.

[29] Kevin Schaal, Andreas Bauer, Praveen Chandrashekar, Rüdiger Pakmor, Christian Klingenberg, and Volker Springel. Astrophysical hydrodynamics with a high-order discontinuous galerkin scheme and adaptive mesh refinement. *Monthly Notices of the Royal Astronomical Society*, 453(4):4278–4300, 2015.